The Environment-Dependent Behavior of the Blatter Radical at the Metal-Molecule Interface

Jonathan Z. Low[a,⊥], Gregor Kladnik[b,c,⊥], Laerte L. Patera[d], Sophia Sokolov[d], Giacomo Lovat[e], Elango Kumarasamy[a], Jascha Repp[d], Luis M. Campos*[,a], Dean Cvetko*[,b,c,f], Alberto Morgante*[,c,g], Latha Venkataraman*[,a,e]

[a]Department of Chemistry, Columbia University, New York, New York 10027, United States

[b]Faculty of Mathematics and Physics, University of Ljubljana, 1000 Ljubljana, Slovenia

[c]CNR-IOM Laboratorio Nazionale TASC, Basovizza, SS-14, km 163.5, I-34012 Trieste, Italy

[d]Institute of Experimental and Applied Physics, University of Regensburg, 93053 Regensburg, Germany

[e]Department of Applied Physics and Applied Mathematics, Columbia University, New York, New York 10027, United States

[f]J. Stefan Institute, Jamova 39, SI-1000 Ljubljana, Slovenia

[g]Department of Physics, University of Trieste, 34127 Trieste, Italy

[⊥]Both authors contributed equally to this work.

ABSTRACT

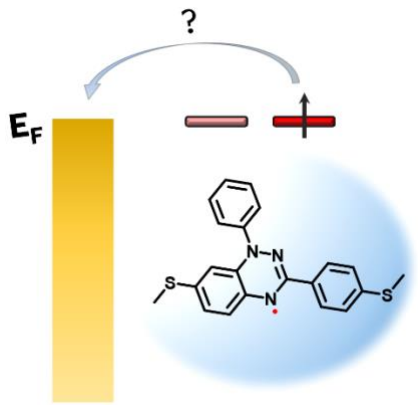

Stable organic radicals have potential applications for building organic spintronic devices. To fulfill this potential, the interface between organic radicals and metal electrodes must be well characterized. Here, through a combined effort that includes synthesis, scanning tunneling microscopy, X-ray spectroscopy and single-molecule conductance measurements, we comprehensively probe the electronic interaction between gold metal electrodes and a benchtop stable radical – the Blatter radical. We find that in spite of its open-shell character and having a half filled orbital close to the Fermi level, the radical is stable on a gold substrate under ultra-high vacuum. We observe a Kondo resonance arising from the radical and spectroscopic signatures from its half-filled orbitals. By contrast, in solution-based single molecule conductance measurements, the radical character is lost through oxidation, with charge transfer occurring from the molecule to metal. Our experiments show that the stability of radical states can be very sensitive to the environment around the molecule.

KEYWORDS: *organic spintronics, organic radicals, Blatter radical, spinterface, Kondo resonance, single-molecule junctions*

INTRODUCTION

Organic radicals are open-shell systems that contain one unpaired electron, making them ideal organic materials for spintronics applications.[1-8] This class of materials can potentially be incorporated into the next generation of memory devices that will consume less power, or even serve as qubits in quantum computing devices.[5-8] Typically, organic radicals are transient species and must be stabilized either by protecting the reactive site sterically or through electronic delocalization of the lone electron.[9-11] However, less is known about the stability of radicals when interfaced with conducting electrodes and metal substrates. The rich variety of radicals and substrates available ensures that there is much interfacial physics and chemistry to explore. Several groups have already demonstrated that these types of molecules can be imaged by scanning tunneling microscopy (STM).[12-16] Some of these studies included observations of a Kondo resonance, arising from the scattering of conduction electrons interacting with the unpaired spin of the radical.[12-14] Furthermore, stable radicals are also amenable to various other spectroscopic studies to probe their electronic structure on different substrates. For example, the sterically protected perchlorinated triphenylmethyl (PTM) radicals retain their radical character on a variety of configurations and surfaces,[2,17] and the radical states can be probed by X-ray spectroscopy.[18] Even electronically stabilized (2,2,6,6-Tetramethylpiperidin-1-yl)oxyl (TEMPO)[19] and nitronyl-nitroxide[20-22] based radicals are stable to X-ray irradiation. These three classes of radicals have therefore been exploited for performing single molecule transport measurements. Molecular junctions formed with PTM radicals can also show Kondo resonances[23] and enhanced conductance[24], while TEMPO and nitronyl-nitroxide based junctions have demonstrated positive[25] and negative[26] magnetoresistance respectively. In these systems, the singly occupied molecular orbitals (SOMOs) of the radicals are all localized at specific sites of the molecule. These orbitals are therefore not strongly coupled to the electrodes.

One class of radicals with large, delocalized SOMOs are 1,2,4-benzotriazin-4-yl radicals (Figure 1a). The first example of a benzotriazinyl radical was synthesized by Blatter in 1968,[27] and now bears his name. The lone electron is not confined to the nitrogen as depicted in Figure 1a but delocalizes across both the triazinyl ring and the fused benzene. This radical is extraordinarily stable and can be stored in ambient conditions for months; some derivatives can persist for even longer.[28] Much credit must go to Koutentis and Constantinides for developing a rich variety of methods to synthesize a library of related compounds as well as studying some of their electronic and magnetic properties, paving the way for this radical to be used in organic electronics.[28-33] Indeed, one of the earliest reports of the Blatter radical was its use as a pressure sensitive semiconductor in a charge transfer complex with TTF.[34] More recently, Ciccullo et al. explored the possibility of using a Blatter derivative as an organic magnet, showing that it is feasible to create thin films that retain their radical properties because the molecule is only weakly physisorbed on the insulating SiO_2 substrate.[35] Crucially, their report demonstrated that the triazinyl radical moiety can also be probed by X-ray spectroscopy without being severely damaged.

Here, we explore the electronic characteristics of the Blatter radical bound to gold by characterizing the metal-molecule interface and measuring its single-molecule transport properties. We present the first images taken of a Blatter radical derivative by scanning tunneling microscopy (STM). Concurrently, scanning tunneling spectroscopy (STS) revealed the presence of a Kondo resonance that arises due to conducting electrons scattering off the unpaired radical electron. We further probe the electronic structure of the molecule through X-ray photoelectron spectroscopy (XPS) and near edge X-ray absorption fine structure (NEXAFS) measurements. This series of experiments performed under ultra-high vacuum (UHV) conditions all confirm that the Blatter radical retains its open-shell radical character upon adsorption onto the Au(111) substrate (Figure 1c). By contrast, in solution-based single metal-molecule-metal junction conductance measurements performed using the scanning tunneling microscope break junction (STM-BJ) method,[36,37] electron transfer occurs from molecule to metal and the radical is oxidized (Figure 1d). These results highlight the importance of the environment on the stability of an open-shell system interacting with a metal electrode.

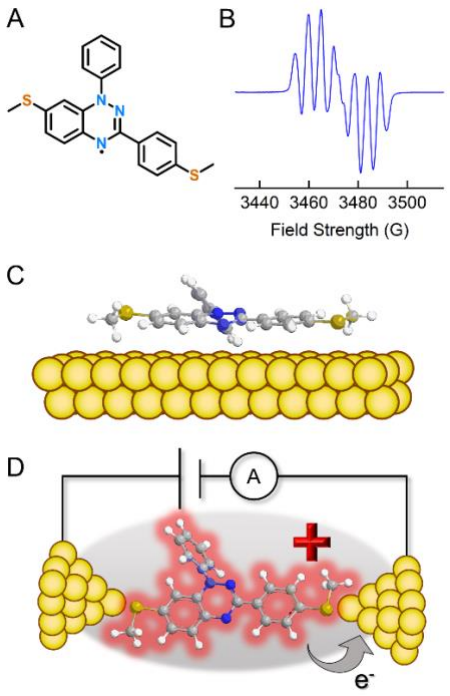

Figure 1. (a) The structure of the Blatter radical studied in this work. (b) EPR spectrum of the Blatter radical in toluene solution. (c) Illustration of the radical deposited on gold in ultra-high vacuum. (d) Illustration of a single-molecule junction where the molecule is positively charged.

RESULTS AND DISCUSSION

We synthesized a novel derivative of the Blatter radical with two gold-binding thiomethyl groups (Figure 1a) according to a reported procedure as detailed in the supporting information (SI).[29]

The electron paramagnetic resonance (EPR) spectrum of the molecule in toluene solution shows the expected 7 line splitting pattern (Figure 1b) due to the unpaired electron coupling to the 3 nitrogen nuclei which each have spin $I = 1$.[28] STM and STS measurements were carried out under UHV conditions (pressure $\approx 5\times10^{-11}$ mbar) at 6.1 K (details in SI). A sub-monolayer coverage of molecules was deposited onto the Au(111) sample kept at about 7 K. For the X-ray spectroscopic measurements, films of the radical were created by evaporating the molecule onto a pristine Au(111) surface in UHV (see SI for details). By controlling the evaporation time and substrate temperature, either a monolayer or a multilayer could be obtained. The terminal thiomethyl groups allow the molecule to bind to the gold electrodes for the STM-BJ measurements performed in solution. Density functional theory (DFT) calculations (details in SI) were used to support our experimental observations.

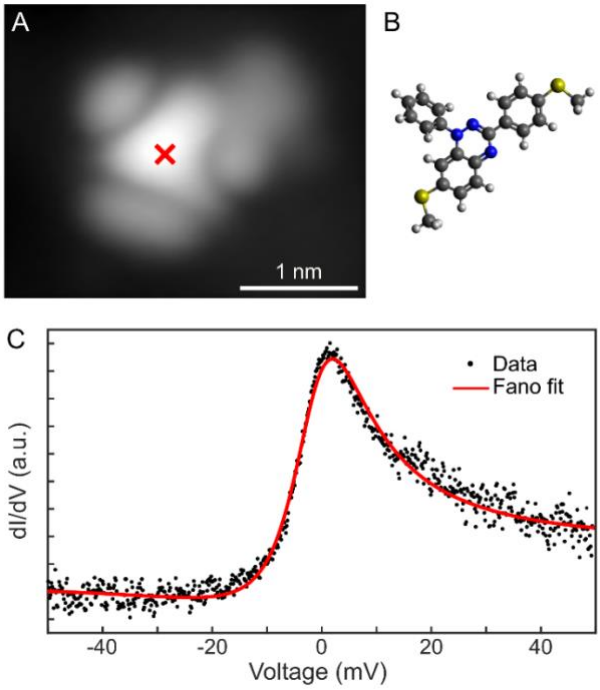

Figure 2. (a) STM image of a single Blatter molecule [$V = 5$ mV; $I = 1.9$ pA]. (b) Molecular model oriented as in (a). (c) dI/dV spectrum taken at the point marked by a red cross on (a), with a superimposed Fano fit.

Figure 2a shows a STM image of an individual Blatter molecule at low coverage. The molecule adsorbs with the benzotriazinyl core (bright part in the center in Figure 2a) lying parallel to the surface. A comparison with the corresponding model in Figure 2b shows that other key features such as the two pendant phenyl rings and thiomethyl groups are visible. A dI/dV spectrum at the point marked by the cross in Figure 2a reveals a clear zero bias peak, resembling a Kondo resonance. By fitting this data with a Fano curve, we determine a coupling strength Γ of 16.8 meV. Following the widely used approach introduced by Nagaoka et al.,[38] the Kondo temperature (T_K) can be estimated to be 43 K. An improved expression of T_K for strongly correlated metal-molecule junctions has been recently proposed by Appelt et al.,[39] which in our case provides a T_K of 83 K. The values obtained with the two different

approaches are both close to the ones reported for other organic radicals (e.g. 37 K for nitrogen-based verdazyl radicals[12] and 54 K for triarylmethyl radicals[13]). The Kondo resonance arises from the presence of an unpaired electron in the molecule; below the Kondo temperature, this unpaired spin interacts with the substrate's continuum of states at the Fermi level, resulting in a sharp Fano-shaped peak at 0 eV.[40] This peak thus provides direct evidence of the retained radical character of the Blatter molecule upon adsorption on gold.

To further investigate the electronic structure of the deposited radical molecules, we turned to X-ray spectroscopy. First, we performed XPS measurements that are sensitive to the electronic and chemical environment around the atoms present in the radical. The wide energy range XPS (Figure S1) shows the expected peaks in the nitrogen 1s (N 1s), carbon 1s (C 1s), and sulfur 2p (S 2p) binding energy regions, with the peak shapes shown in Figure S2. Figure 3a shows the high-resolution signal around the N 1s region of both the monolayer and multilayer films. These can be fit to 3 main peaks with a 1:1:1 ratio, corresponding to the 3 distinct nitrogen atoms as assigned by Ciccullo et al.,[35] and also corroborated with our DFT calculations (Figure S3). The peaks in the monolayer are shifted toward slightly lower binding energies due to stronger screening from the gold substrate. The presence of the lowest binding energy peak at 398.7 eV in the multilayer indicates that the radical nitrogen (N4, Figure 3a inset) is intact and this derivative of the Blatter radical retains its unpaired electron when deposited through thermal desorption; this peak diminishes when the radical suffers beam damage (vide infra and in the SI). The other two peaks that occur shifted higher by 1.0 eV and 2.8 eV in the multilayer are assigned to N2 and N1 respectively as indicated in Figure 3a. The XPS of the multilayer also has additional features – a small peak at the high binding energy side of the spectrum (dashed line) which is assigned to shake-up transitions,[35] as well as a secondary doublet that consists of peaks in a 2:1 ratio (indicated in light gray). We ascribe the secondary doublet to a species that arises from beam damage to the pristine molecules, as detailed in the SI (and Figure S4). The monolayer spectrum has also been fit with additional peaks (in light gray) which could be due to impurities or beam damage.

Next, we examine the N 1s (K-edge) NEXAFS spectra which probes the electronic structure of the unoccupied states and can therefore elucidate the existence of a singly unoccupied molecular orbital (SUMO) which should be present if the open-shell structure is unperturbed. Figure 3b shows the N 1s NEXAFS spectrum of the multilayer sample in black, with the monolayer in blue. In both spectra, there are 3 peaks in this region – 2 smaller peaks and a taller one – which arise from electronic transitions from the N 1s core to the lowest unoccupied states in the radical. To assign these peaks, we turn to DFT calculations of the NEXAFS spectrum as detailed in the SI (and Figure S5). The peaks at 396.8, 397.8 and 399.7 eV indicated by the green arrows on the multilayer NEXAFS follow the same energy spacing as the 3 N 1s XPS peaks. These peaks correspond to transitions from 3 different atoms (N4, N2, and N1 respectively) into the π^* SUMO, since this orbital has significant electron density on all three nitrogen atoms. A schematic of these transitions, along with the calculated molecular orbitals are shown

in Figures 3c and 3d. The 399.7 eV peak has a higher intensity because it overlaps with a second peak, visible as a shoulder and indicated by the orange arrow on the spectrum of the multilayer. This shoulder peak can be assigned to a transition from the 1s level of one N atom to the next unoccupied π* orbital (the first doubly-unoccupied LUMO). There is only a single peak because this orbital has significant electron density only on the N2 atom (Figure 3d). The peaks in the monolayer NEXAFS can be assigned to the same transitions. Although the shoulder peak is not as well-resolved in the monolayer spectrum, it still adds intensity to the N1 peak. Another key feature of the monolayer NEXAFS is that changing the photon linear polarization from perpendicular to the surface (*p*-pol) to almost parallel to the surface (*s*-pol) attenuates the 3 peaks in the 396 – 400 eV range (Figure S6), confirming that the molecule lies mostly flat on gold in both the X-ray and STM setups while retaining its radical character.[41]

The similarity of the XPS and NEXAFS spectra in both films shows that whether the radical is in direct contact with the gold substrate (as when in a monolayer) or is only interacting with layers of other molecules below it (as in the multilayer), the radical character is not lost. This result dovetails nicely with the observation of the Kondo resonance from STS measurements, corroborating that the Kondo peak observed arises from the unpaired electron.

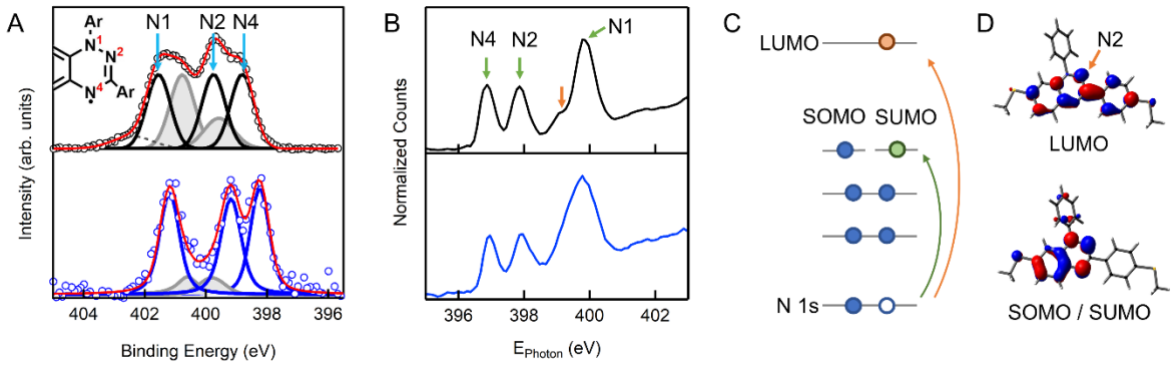

Figure 3. (a) Nitrogen 1s XPS spectra of the multilayer (top, black) and monolayer (bottom, blue) along with the fits. For the multilayer, peaks are assigned to the nitrogen atoms as indicated and a partial structure of the Blatter radical with the nitrogen atoms labelled is shown in the inset. The shaded light gray peaks in the multilayer spectrum are due to a second, damaged species present in the sample (details in main text and SI). (b) Nitrogen 1s NEXAFS spectra of a multilayer (black) and monolayer (blue) of the Blatter radical derivative. The peaks are labelled by the individual nitrogen atoms that cause the absorption features. (c) Schematic of the electronic transitions associated with the NEXAFS peaks. The green and orange arrows show the transitions corresponding to the peaks indicated in (b). (d) The frontier unoccupied orbitals involved in the transitions described in (c), obtained from gas-phase DFT calculations. Note that in the DFT of the radical, the α and β spin orbitals are treated separately and only the α orbitals are shown in here. The β orbitals are qualitatively similar and can be found in Figure S7.

We now turn to solution based single molecule conductance measurements carried out using the STM-BJ method.[36,37] In this method, a gold STM tip is driven into contact with a gold substrate and slowly retracted while in a solution of molecules with gold binding groups. A small bias is applied between the tip and substrate, and the conductance is recorded as a function of relative tip/substrate

displacement. As the tip is withdrawn, a gold-gold point contact with a conductance around 1 G_0 (= $2e^2/h$ = 77.48 μS) is formed. Further retraction of the tip breaks the gold point contact and a molecule can bind between the electrodes, creating plateaus below the 1 G_0 feature in the conductance versus displacement graphs. These plateaus are the conductance signatures of individual molecular junctions. The data from thousands of individual traces can be collected and compiled into logarithmically binned 1D conductance histograms to identify the conductance peaks (Figure 4a). No data selection is performed.

The 1D histogram of the Blatter radical is shown as the brown trace in Figure 4a. Two clear conductance features are visible – a sharp, high conductance peak at around 3.2×10^{-3} G_0, and a broad peak near 3.2×10^{-5} G_0 which is ~100 times lower in conductance. In the 2D conductance histogram which is created by overlaying the individual conductance versus displacement traces (Figure 4b), the lower conductance peak is slightly offset to longer displacements than the high conductance peak, indicating that this low conductance feature appears only after the tip is retracted further and the high conductance plateau ruptures. We attribute the higher conductance peak to a molecular junction with both thiomethyl linkers bound to the gold electrodes, while the lower conductance peak is a dimer junction where only one end of each molecule binds to the gold electrode and conduction occurs through the interaction of the two π systems.[42-44] The nature of the two peaks was established by analyzing conductance noise according to a previously reported method and detailed in the SI (Figures S8-10).

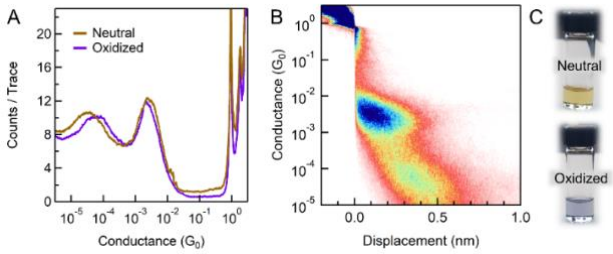

Figure 4. (a) 1D conductance histogram of the neutral radical (brown) and chemically oxidized radical (purple) measured at 200 mV and compiled from 3000 traces. (b) 2D conductance histogram of the neutral radical created from the same traces used for the 1D histogram shown in (a). (c) Photos of the different colored solutions of the neutral and oxidized species.

Surprisingly, the high conductance peak of the radical is very similar in magnitude to that of 4,4'-di(methylthio)stilbene (Figure S11). Both these molecules have 11 bonds along the conductance pathway. This result is contrary to the expectation that the conductance of an open-shell radical should be high due to the availability of a low-lying orbital for electron transfer.[45] Since the Blatter derivative has a conductance similar to that of a closed-shell stilbene, we hypothesized that the radical loses its open-shell character in a single-molecule junction. We therefore tested the redox stability of the radical in solution by performing cyclic voltammetry (CV) in the STM-BJ setup (details in SI). Figure S12

shows that with gold electrodes, the molecule is oxidized at very low potentials. The reduction wave, although visible in the platinum electrode CV (Figure S13), is never observed in the voltammogram recorded on gold. This led us to investigate the conductance of a chemically oxidized Blatter radical derivative.

We performed the STM-BJ measurement with a solution of the chemically oxidized Blatter derivative (details in the SI). The solution of the radical turns from brown to purple upon oxidation (Figure 4c), and it can be characterized by UV-Vis and NMR spectroscopy as it is a closed-shell species (Figures S14 and S15). The conductance histogram of the oxidized species is the purple trace in Figure 4a, which is nearly identical to the histogram of the neutral radical. This strongly suggests that the neutral radical gets oxidized spontaneously when bound in a junction, and the conductance traces generated are that of the closed-shell oxidized species. We stress that the oxidation only occurs in the junction at the metal-molecule interface, since the color of the solution of neutral molecules is the same before and after the experiment.

Clearly, the chemical behavior of the Blatter radical in the STM-BJ measurements is very different from what was observed in the STS, XPS and NEXAFS. Under UHV conditions, the molecule unambiguously retains its radical character. On the other hand, in a junction with the molecule bound to two electrodes, the radical is spontaneously oxidized instead, readily losing the electron in its SOMO. To reconcile the different behavior of the radical on gold in two different environments, we consider two key differences between the UHV and STM-BJ measurements. First, the level alignment at the interface is likely to be very sensitive to the environment; the SOMO could thus be slightly higher than the Fermi energy of gold in a molecular junction in solution, allowing for facile molecule-to-metal charge transfer. Second, undercoordinated gold adatoms which the molecules bind to in the STM-BJ (Figure 1d) are slightly electron deficient;[46,47] this could also facilitate the oxidation of a low-lying SOMO.

CONCLUSION

In conclusion, we have investigated how the Blatter radical interacts with gold electrodes. STS, XPS and NEXAFS measurements show that the radical character is not affected upon adsorption on the Au(111) surface in UHV, such that the molecule retains its open shell configuration. In single molecule conductance measurements performed in solution, we demonstrate that the conductance signature arises from an oxidized radical. We propose that this behavior stems from the proximity of the SOMO to the Fermi level of gold because in such cases, small changes in the surrounding conditions can shift the alignment of the molecular orbitals. Our work shows that radicals with their half-filled orbitals close to the Fermi level can behave very differently even with the same substrate under different environments, thereby illustrating the importance of metal-molecule coupling to the stability of radicals on metal surfaces.

ASSOCIATED CONTENT

Supporting information

The supporting information, which includes synthesis and characterization of the molecules together with additional experimental figures and discussion is available free of charge at _____.

AUTHOR INFORMATION

Corresponding Authors

*E-mail: lv2117@columbia.edu

*E-mail: morgante@iom.cnr.it

*E-mail: cvetko@iom.cnr.it

*E-mail: lcampos@columbia.edu

Notes

The authors declare no competing financial interest.

ACKNOWLEDGMENTS

The experimental work was supported primarily by the National Science Foundation (award number DMR-1507440 and DMR-1807580). G.L. thanks the Center for Precision Assembly of Superstratic and Superatomic Solids at Columbia University, an NSF MRSEC (award number DMR-1420634) for funding. Gas phase DFT calculations used the Extreme Science and Engineering Discovery Environment (XSEDE) startup allocation TG-DMR150018. XSEDE is supported by NSF grant number ACI-1548562.[48] J.Z.L. thanks the A*STAR Graduate Academy in Singapore for a graduate fellowship. D.C. and G.K. acknowledge partial financial support from the Slovenian Research Agency (program number P1-0112). G.K. acknowledges financial support from the SIR grant SUNDYN (Nr. RBSI14G7TL, CUP B82I15000910001) of the Italian Ministry of Education, Universities and Research MIUR. We thank Steffen Jockusch for performing EPR spectroscopy and Brandon Fowler for mass spectrometry. L.L.P., S.S. and J.R. acknowledge financial support from the Deutsche Forschungsgemeinschaft (through CRC 1277 - B01 and project RE2669/6-1).

REFERENCES

(1) Sanvito, S. *Chem. Soc. Rev.* **2011**, *40*, 3336-3355.

(2) Mas-Torrent, M.; Crivillers, N.; Rovira, C.; Veciana, J. *Chem. Rev.* **2012**, *112*, 2506-2527.

(3) Mas-Torrent, M.; Crivillers, N.; Mugnaini, V.; Ratera, I.; Rovira, C.; Veciana, J. *J. Mater. Chem.* **2009**, *19*, 1691-1695.

(4) Herrmann, C.; Solomon, G. C.; Ratner, M. A. *J. Am. Chem. Soc.* **2010**, *132*, 3682-3684.

(5) Yonekuta, Y.; Susuki, K.; Oyaizu, K.; Honda, K. *J. Am. Chem. Soc.* **2007**, *129*, 14128-14129.

(6) Lee, J.; Lee, E.; Kim, S.; Bang, G. S.; Shultz, D. A.; Schmidt, R. D.; Forbes, M. D. E.; Lee, H. *Angew. Chem., Int. Ed.* **2011**, *50*, 4414-4418.

(7) McGuire, J.; Miras, H. N.; Donahue, J. P.; Richards, E.; Sproules, S. *Chem. - Eur. J.* **2018**, *24*, 17598-17605.

(8) McGuire, J.; Miras, Haralampos N.; Richards, E.; Sproules, S. *Chem. Sci.* **2019**, *10*, 1483-1491.

(9) Hicks, R. G. *Org. Biomol. Chem.* **2007**, *5*, 1321-1338.

(10) Ratera, I.; Veciana, J. *Chem. Soc. Rev.* **2012**, *41*, 303-349.

(11) Campos, L. M.; Garcia-Garibay, M. A. In *Reviews of Reactive Intermediate Chemistry*; Platz, M. S., Moss, R. A., Jones Jr., M., Eds.; John Wiley & Sons, Inc.: New Jersey, USA, 2007, p 271-331.

(12) Liu, J.; Isshiki, H.; Katoh, K.; Morita, T.; Breedlove, B. K.; Yamashita, M.; Komeda, T. *J. Am. Chem. Soc.* **2013**, *135*, 651-658.

(13) Müllegger, S.; Rashidi, M.; Fattinger, M.; Koch, R. *J. Phys. Chem. C* **2013**, *117*, 5718-5721.

(14) Zhang, Y.-h.; Kahle, S.; Herden, T.; Stroh, C.; Mayor, M.; Schlickum, U.; Ternes, M.; Wahl, P.; Kern, K. *Nat. Commun.* **2013**, *4*, 2110.

(15) Grillo, F.; Mugnaini, V.; Oliveros, M.; Francis, S. M.; Choi, D.-J.; Rastei, M. V.; Limot, L.; Cepek, C.; Pedio, M.; Bromley, S. T.; Richardson, N. V.; Bucher, J.-P.; Veciana, J. *J. Phys. Chem. Lett.* **2012**, *3*, 1559-1564.

(16) Grillo, F.; Fruchtl, H.; Francis, S. M.; Mugnaini, V.; Oliveros, M.; Veciana, J.; Richardson, N. V. *Nanoscale* **2012**, *4*, 6718-6721.

(17) Bejarano, F.; Olavarria-Contreras, I. J.; Droghetti, A.; Rungger, I.; Rudnev, A.; Gutiérrez, D.; Mas-Torrent, M.; Veciana, J.; van der Zant, H. S. J.; Rovira, C.; Burzurí, E.; Crivillers, N. *J. Am. Chem. Soc.* **2018**, *140*, 1691-1696.

(18) Mugnaini, V.; Calzolari, A.; Ovsyannikov, R.; Vollmer, A.; Gonidec, M.; Alcon, I.; Veciana, J.; Pedio, M. *J. Phys. Chem. Lett.* **2015**, *6*, 2101-2106.

(19) Arantes, C.; Chernick, E. T.; Gruber, M.; Rocco, M. L. M.; Chassé, T.; Tykwinski, R. R.; Casu, M. B. *J. Phys. Chem. C* **2016**, *120*, 3289-3294.

(20) Kakavandi, R.; Savu, S.-A.; Caneschi, A.; Casu, M. B. *J. Phys. Chem. C* **2013**, *117*, 26675-26679.

(21) Savu, S.-A.; Biswas, I.; Sorace, L.; Mannini, M.; Rovai, D.; Caneschi, A.; Chassé, T.; Casu, M. B. *Chem. - Eur. J.* **2013**, *19*, 3445-3450.

(22) Kakavandi, R.; Savu, S.-A.; Sorace, L.; Rovai, D.; Mannini, M.; Casu, M. B. *J. Phys. Chem. C* **2014**, *118*, 8044-8049.

(23) Frisenda, R.; Gaudenzi, R.; Franco, C.; Mas-Torrent, M.; Rovira, C.; Veciana, J.; Alcon, I.; Bromley, S. T.; Burzurí, E.; van der Zant, H. S. J. *Nano Lett.* **2015**, *15*, 3109-3114.

(24) Yuan, L.; Franco, C.; Crivillers, N.; Mas-Torrent, M.; Cao, L.; Sangeeth, C. S. S.; Rovira, C.; Veciana, J.; Nijhuis, C. A. *Nat. Commun.* **2016**, *7*, 12066.

(25) Hayakawa, R.; Karimi, M. A.; Wolf, J.; Huhn, T.; Zöllner, M. S.; Herrmann, C.; Scheer, E. *Nano Lett.* **2016**, *16*, 4960-4967.

(26) Sugawara, T.; Minamoto, M.; Matsushita, M. M.; Nickels, P.; Komiyama, S. *Phys. Rev. B* **2008**, *77*, 235316.

(27) Blatter, H. M.; Lukaszewski, H. *Tetrahedron Lett.* **1968**, *9*, 2701-2705.

(28) Constantinides, C. P.; Koutentis, P. A.; Krassos, H.; Rawson, J. M.; Tasiopoulos, A. J. *J. Org. Chem.* **2011**, *76*, 2798-2806.

(29) Koutentis, P. A.; Lo Re, D. *Synthesis* **2010**, *12*, 2075-2079.

(30) Berezin, A. A.; Zissimou, G.; Constantinides, C. P.; Beldjoudi, Y.; Rawson, J. M.; Koutentis, P. A. *J. Org. Chem.* **2014**, *79*, 314-327.

(31) Constantinides, C. P.; Obijalska, E.; Kaszyński, P. *Org. Lett.* **2016**, *18*, 916-919.

(32) Karecla, G.; Papagiorgis, P.; Panagi, N.; Zissimou, G. A.; Constantinides, C. P.; Koutentis, P. A.; Itskos, G.; Hayes, S. C. *New J. Chem.* **2017**, *41*, 8604-8613.

(33) Savva, A. C.; Mirallai, S. I.; Zissimou, G. A.; Berezin, A. A.; Demetriades, M.; Kourtellaris, A.; Constantinides, C. P.; Nicolaides, C.; Trypiniotis, T.; Koutentis, P. A. *J. Org. Chem.* **2017**, *82*, 7564-7575.

(34) Hutchison, K.; Srdanov, G.; Menon, R.; Gabriel, J.-C.; Knight, B.; Wudl, F. *Synth. Met.* **1997**, *86*, 2147-2148.

(35) Ciccullo, F.; Gallagher, N. M.; Geladari, O.; Chassé, T.; Rajca, A.; Casu, M. B. *ACS Appl. Mater. Interfaces* **2016**, *8*, 1805-1812.

(36) Xu, B.; Tao, N. J. *Science* **2003**, *301*, 1221-1223.

(37) Venkataraman, L.; Klare, J. E.; Tam, I. W.; Nuckolls, C.; Hybertsen, M. S.; Steigerwald, M. L. *Nano Lett.* **2006**, *6*, 458-462.

(38) Nagaoka, K.; Jamneala, T.; Grobis, M.; Crommie, M. F. *Phys. Rev. Lett.* **2002**, *88*, 077205.

(39) Appelt, W. H.; Droghetti, A.; Chioncel, L.; Radonjić, M. M.; Muñoz, E.; Kirchner, S.; Vollhardt, D.; Rungger, I. *Nanoscale* **2018**, *10*, 17738-17750.

(40) Scott, G. D.; Natelson, D. *ACS Nano* **2010**, *4*, 3560-3579.

(41) Stöhr, J. In *NEXAFS Spectroscopy*; Springer Berlin Heidelberg: Berlin, Heidelberg, 1992, p 276-291.

(42) Wu, S.; Gonzalez, M. T.; Huber, R.; Grunder, S.; Mayor, M.; Schonenberger, C.; Calame, M. *Nat. Nanotechnol.* **2008**, *3*, 569-574.

(43) Frisenda, R.; Janssen, V. A. E. C.; Grozema, F. C.; van der Zant, H. S. J.; Renaud, N. *Nat. Chem.* **2016**, *8*, 1099.

(44) Magyarkuti, A.; Adak, O.; Halbritter, A.; Venkataraman, L. *Nanoscale* **2018**, *10*, 3362-3368.

(45) Heimel, G.; Zojer, E.; Romaner, L.; Brédas, J.-L.; Stellacci, F. *Nano Lett.* **2009**, *9*, 2559-2564.

(46) Mielke, J.; Hanke, F.; Peters, M. V.; Hecht, S.; Persson, M.; Grill, L. *J. Am. Chem. Soc.* **2015**, *137*, 1844-1849.

(47) Smoluchowski, R. *Phys. Rev.* **1941**, *60*, 661-674.

(48) Towns, J.; Cockerill, T.; Dahan, M.; Foster, I.; Gaither, K.; Grimshaw, A.; Hazlewood, V.; Lathrop, S.; Lifka, D.; Peterson, G. D.; Roskies, R.; Scott, J. R.; Wilkins-Diehr, N. *Comput. Sci. Eng.* **2014**, *16*, 62-74.